Assessing Power and Water Network Resilience When Water Pumps Provide Frequency Regulation

Anna Stuhlmacher *Member, IEEE*, Seth Guikema, and Johanna L. Mathieu *Senior Member, IEEE*

***Abstract*—Pumps in drinking water distribution networks can be operated as flexible, controllable loads to help support the electric power grid, e.g., by providing frequency regulation. However, departures from conventional water network operation should not degrade the ability of the water and power networks to respond to high impact low frequency events. In this paper, we evaluate the resilience of water and power distribution networks surrounding a storm-induced power outage given an optimal pumping strategy that minimizes electricity costs and is capable of offering frequency regulation. The water network resilience under optimal water pumping strategies is compared with its resilience under a conventional rule-based water pumping strategy. In a case study, we consider an extreme wind event that causes power outages in the power distribution network impacting pumps in the water network. We found that the optimal control strategies are significantly less expensive than the traditional rule-based strategy but the water tanks levels are lower within the optimal pumping strategies, potentially reducing water service availability during long power outages. However, we also observed that the tank levels remain further from their limits when the optimal pumping strategy provides frequency regulation in addition to minimizing electricity costs, resulting in improved resilience metrics.**

***Index Terms*—extreme weather, frequency regulation, power distribution network, resilience, water network**

NOMENCLATURE

Sets

$\mathcal{E}$	Water network edges
$\mathcal{J}$	Water network junctions
$\mathcal{K}$	Power distribution network buses
$\mathcal{L}$	Power distribution network lines
$\mathcal{N}$	Water network nodes
$\mathcal{P}$	Water network pumps
$\mathcal{R}$	Water network reservoirs
$\mathcal{S}$	Water network storage tanks
$\mathcal{T}$	Time steps in the scheduling problem

Parameters

A_{c}	Conductor area
b_{ij}^1, b_{ij}^0	Head gain coefficients for pump ij
c	Tank level slack variable penalty coefficient
c_{ij}^1, c_{ij}^0	Pump power parameters of pump ij
d_j^t	Water demand at junction j, time t
$f_{ij}^{t,1}, f_{ij}^{t,0}$	Linearized parameters of edge ij, time t
$\hat{h}_j$	Elevation head of node j
h	Height of utility pole
$\underline{H}_j, \overline{H}_j$	Min., max. head for node j
k_{ij}	Resistance coefficient of pipe ij
N	Number of scenarios
V^t	Three-second gust wind speed at time t
$\underline{w}_{ij}, \overline{w}_{ij}$	Min., max. normalized speed of pump ij
$\overline{x}_{ij}$	Maximum flow rate of pump ij
y	Modified age of the utility pole
γ_j	Cross-sectional area of tank j
ΔT	Duration of time step
θ	Angle between wind direction and conductors
ν	Pipe head loss exponent
π_{ij}^t	Energy price at time t for pump ij, time t
π_{fr}^t	Price of frequency regulation capacity at time t
ϕ	Tank water level tolerance

Decision Variables

$F_{ij}^t \in \boldsymbol{F}$	Frequency regulation capacity of pump ij, time t
H_j^t	Hydraulic head at node j, time t
$p_{ij}^t \in \boldsymbol{p}$	3-phase real power demand of pump ij, time t
s	Tank level slack variable
w_{ij}^t	Normalized speed of pump ij, time t
W_{ij}^t	Normalized speed squared of pump ij, time t
x_{ij}^t	Flow rate of water through pipe ij, time t
z_{ij}^t	On/off status of pump ij, time t

Resilience Metrics

P^t	Network performance at time t
R_n	Network resilience metric of scenario n

Subscripts

FR	Frequency regulation
line	Active lines
load	Connected loads
N	Operation under normal conditions
pressure	Pressure met
tank	Final tank capacity
W	Operation under wind-induced outage conditions
wsa	Water service availability

This work was partially supported by NSF Award 2222096. A. Stuhlmacher is with the Department of Electrical and Computer Engineering, Michigan Technological University, Houghton, MI, USA (e-mail: annastu@mtu.edu). S. Guikema is with the Department of Industrial and Operations Engineering and the Department of Civil and Environmental Engineering, University of Michigan, Ann Arbor, MI, USA (e-mail: sguikema@umich.edu). J.L. Mathieu is with the Department of Electrical Engineering and Computer Science, University of Michigan, Ann Arbor, MI, USA (e-mail: jlmath@umich.edu).

I. INTRODUCTION

As more intermittent renewable energy sources are added to the electric power grid, more sources of flexibility are needed to ensure safe grid operation. There is growing interest in utilizing water pumps in drinking water distribution networks as a source of flexibility for the electric power grid. Pumps in water distribution networks can be treated as flexible loads, capable of shifting their power consumption both temporally (utilizing water storage tanks) and spatially (across multiple

pumping stations). Recent work focuses on optimizing the operation of water distribution networks given the interactions and interconnection between the water network and the electric power grid (for example, to leverage the water network to provide services to the power grid), such as [1]–[10]. In a pilot program, the Pennsylvania American Water utility successfully provided frequency regulation to PJM, resulting in electricity cost savings of 2-3% by adjusting the speed of a single variable speed pump [11]. This pilot program demonstrates the ability of variable speed pumps to adjust on the seconds-scale to provide frequency regulation, and also the value provided by these actions. In [12], the flexibility potential of leveraging drinking water pumps to provide grid services was found to be a sizable asset. The estimated power and energy capacity was around 21 GW and 925 GWh in the United States, respectively.

However, we need to ensure that the proposed operational choices do not degrade the resilience of the networks compared to the resilience of conventionally implemented practices. Most water distribution networks currently operate using heuristic control rules that adjust pump and valve settings given time patterns or events (e.g., triggered by tank water level and/or nodal pressures). In this work, we investigate the performance of the water distribution network before, during, and after a storm-induced power outage when the supply pumps are optimally scheduled and controlled to provide grid services.

There is a major focus on resilience in power networks (e.g., [13]–[15]) and in water networks (e.g., [16]) since both networks are considered critical infrastructure systems. However, few papers investigate the resilience across interconnected power and water distribution systems with the exception of [17]–[19], which propose coupled power-water network resilience metrics. These works help capture the interactions between power and water networks. However, to the best of our knowledge, no work considers the impact of optimal water distribution network control on the resilience of power and water distribution networks.

The goal of this paper is to evaluate the operational resilience of the power and water distribution network to hazard events under different water pumping operational strategies. Specifically, we consider optimal water pumping strategies subject to water flow constraints that minimize pump electricity costs and provide frequency regulation to the bulk transmission system. We solve for the pump schedules and frequency regulation capacity bid into the ancillary service market. It should be noted that we are considering frequency regulation (also known as second frequency control or load frequency control) not frequency response (also known as droop control or primary frequency control). Specifically, to provide frequency regulation, the pumps must adjust their power consumption based on a frequency regulation signal sent by the independent system operator. Real-time frequency regulation control actions are determined based on the affinity laws. We then evaluate the strategies within a hydraulic simulation. Metrics (e.g., the number of power distribution lines online and the amount of water demand served) quantify the resilience of the water and power distribution networks after a wind event that causes power outages, and network performance under the optimal pump control strategy is compared with the performance under conventional rule-based water network operation.

Some past approaches have considered water pumping providing frequency regulation, e.g., [5], [20]. In previous work, we considered providing frequency regulation and voltage support concurrently with fixed speed pumps [5]. In contrast, here, we consider variable speed pumps which are better suited to respond to a frequency regulation signal by adjusting their speed set point. In [20], the authors solve for demand response and frequency regulation capacity in a radial 15-node test network using variable speed pumps; however, they do not specify or simulate the real-time pump speed adjustments given a frequency regulation signal, as we do here.

An important aspect of our work is ensuring that optimal water pumping strategies produce tractable and feasible solutions within nonconvex hydraulic simulations. When evaluating some of the existing modeling and approximation approaches within a hydraulic simulator, we observed cases where the tank levels were drained or filled more than expected. This led to cases with infeasible solutions or reduced water service availability. To address this, we improve and extend upon existing optimal water pumping formulations that provide frequency regulation in order for the formulation to apply to variable speed pumps and preserve accuracy. Specifically, we use an iterative mixed integer linear programming approach similar to [21], that incorporates variable speed pumps while using soft tank level constraints to improve convergence. This approach is evaluated in Section V with a high-fidelity hydraulic simulator with two-second time steps.

In summary, the contributions of this work are 1) improving upon optimal water pumping formulations to incorporate variable speed pumps while ensuring tractability and accuracy within the original problem, 2) using a hydraulic simulator to compare the accuracy and performance of the rule-based and optimal water flow strategies under normal and extreme conditions, 3) simulating a wind-based hazard event and investigating the impact of pump control strategies on the water network's operational resilience in a case study, and 4) discussing the implications of our results and how network resilience can be incorporated in optimal water pumping problems.

The rest of this paper is organized as follows: Section II provides an overview of our approach and the considered pump control strategies. In Section III, we present the hazard modeling and simulation methods as well as discuss how we quantify and compare the resilience of the power and water network under different control strategies. The optimal pumping problems are fully described in Section IV. Last, we present the results of a case study in Section V and provide concluding remarks in Section VI.

II. Problem Description

We consider interconnected power and water distribution networks experiencing a wind hazard event that may damage the utility poles in the power distribution network. Underground water distribution systems are indirectly impacted by

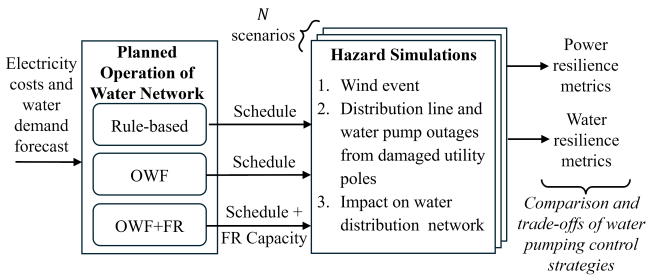

Fig. 1. Flowchart of process.

wind events: power outages in the power distribution network cause water pumping stations to shut down which can lead to reduced water pressures and water shortages in the water distribution network. While power outages impact both the power and water distribution network, power outages do not typically cause long-term damage to the water distribution network [22]. It should be noted that a water distribution network may have fuel-based backup pumps that may eliminate or postpone water delivery issues. However, backup pumps are usually insufficient to meet demand for significant power outages [23].

A. Problem Approach

Figure 1 provides a general outline of our approach to evaluate the resilience of the power and water distribution networks under different operational strategies and power outage scenarios. We first determine the planned pump operation for three different control strategies, which are outlined in Section II-B and formulated in Section IV. Given the planned pump operation, we evaluate the operational resilience of the power and water network experiencing a wind hazard event that damages wooden utility poles. To do this, we simulate N large wind event scenarios and evaluate the power distribution network's (and correspondingly the water distribution network's) vulnerability to the considered hazard under different operational schemes. Probabilistic fragility curves are used to generate N wind hazard event scenarios (see Section III-A). In this paper, we compare how different operational control strategies pre-position a water distribution network to respond to storm-induced power outages. For each wind event scenario, we run hydraulic simulations given the pump outages and restorations. We then compute power and water distribution network resilience metrics for all scenarios. We describe the hydraulic simulator in Section III-B and the resilience metrics in Section III-C.

B. Water Distribution Network Operational Control Strategies

In this work, we evaluate network resilience under three different operational strategies. The operational control strategies are employed under normal operation, or pre-contingency. When the water network is experiencing pump outages, the water system operator would prioritize supplying sufficient water to consumers at adequate water pressures, over minimizing costs.

1) Rule-Based Control (Rule): We compare our optimal pumping strategies against the rule-based controls that are traditionally used by water system operators. Control rules in EPANET can adjust the status and setting of pumps and valves based on simulation time triggers (e.g., turn pump 2 off at 5:00 am) or network conditions (e.g., turn on pump 1 if the tank pressure goes below five meters).

2) Optimal Water Flow Control (OWF): We optimally solve for the water pump operation subject to the water flow constraints while minimizing water pumping electricity costs. We formulate this problem as a mixed-integer linear program that we solve iteratively, which is described in Section IV-B.

3) Optimal Water Flow Control + Frequency Regulation (OWF+FR): We optimize the water pump operation to provide frequency regulation subject to the water flow constraints. We minimize the operational costs, i.e., the electricity cost of pump power consumption minus the profit associated with providing frequency regulation capacity. We solve for the pump schedule and frequency regulation capacity that can be provided in the ancillary service market over a 24-hour scheduling horizon. In real time, we adjust the pump speed to respond to the frequency regulation signal using the affinity laws. The OWF+FR formulation and the frequency regulation signal adjustments are described in Section IV-C.

III. Wind Hazard Event Modeling and Simulation

In this section, we first describe modeling wind hazard events and the subsequent damage states of the wooden utility poles in the power distribution network. We then describe the hydraulic simulator and the metrics used to evaluate the resilience of the power and water networks.

A. Hazard Simulation and Outage States

We consider a multi-period wind event that can damage wooden utility poles. The damage states of the wooden utility poles determine the outage statuses of the lines and buses within the power distribution network as well as the power outage statuses of the water pumps. We consider N scenarios, or replications, of a wind hazard event in order to evaluate the resilience of the networks under a range of damage state outcomes. Below are the steps used to generate the outage states of the power and water distribution networks given a wind event.

1) Wind-based Hazard Event: For each scenario, the start time of the wind event is randomly generated from a uniform distribution. This allows us to consider the impact of hazards occurring at different times during the simulation horizon. Similar to [15], we assume time-varying, deterministic wind speeds that are uniform over the entire power distribution network. It should be noted that we could also simulate the wind fields with spatial resolution, e.g., [24].

2) Fragility Curves: For each scenario, we determine the damage states of the wooden utility poles in the power distribution network using fragility curves. A fragility curve is a probabilistic analysis of a specific network component's performance under extreme conditions (see Fig. 2). For instance, a wooden utility pole can have a probability of failure

from zero (unaffected) to one (critical, 100% chance of failure) given the wind speed intensity. We use the fragility curves of wooden utility poles for strong wind events developed in [25]. A utility pole's probability of failure during wind events is estimated given information on the poles (class, age, and height), conductors (number, diameter, orientation, and span length), and wind (speed and direction) [25]. The fragility curve is modeled with a lognormal cumulative distribution function

$$P_f(V^t, y, \theta, A_c, h) = \Phi\left(\frac{\ln(2.24V^t) - \mu(y, \theta, A_c, h)}{\sigma(y, \theta, A_c, h)}\right), \quad (1)$$

where P_f is the probability of failure (-), V^t is the three-second gust wind speed at time step t (m/s), y is the modified age of the pole (years), θ is the angle between the wind direction and the conductors (degrees), A_c is the conductor area (m^2), h is the height of pole (m), and $\Phi(\cdot)$ is the cumulative distribution function of the standard normal distribution. The second-degree multivariable functions $\mu(\cdot)$ and $\sigma(\cdot)$ return the mean and standard deviation of the lognormal distribution, where the coefficients are fitted for different pole classes given 20,000 training points in [25]. It should be noted that the fragility curve in [25] does not depict the full damage impact of wind events on the power distribution network, since it does not consider downed lines from vegetation and debris.

3) Utility Pole Damage Scenarios: We next create N multi-period scenarios given the fragility curves, where each scenario includes the damage states for all utility poles over the scheduling horizon. Given the span length and the distance between buses in the power distribution network topology, we determine the number of wooden utility poles between connected buses. For each scenario, we determine which (if any) utility poles are damaged during the wind hazard event. A pole fails at time t if $P_f(V^t, y, \theta, A_c, h) > r^t$, where $r^t \in [0, 1]$ is randomly generated from a uniform distribution. We consider a finite number of repair crews, where the poles within the power distribution network are repaired in order of importance. In other words, there is a priority to get critical infrastructure, such as water pumps, online first. The water distribution network is considered critical infrastructure and is essential for providing clean drinking water to consumers. Long pump outages and inadequate pressure levels can lead to contamination, boil water advisories, and water shortages.

4) Network Outage Scenarios: Given the utility pole damage states in the N scenarios, we determine what distribution lines and water pumps are experiencing outages.

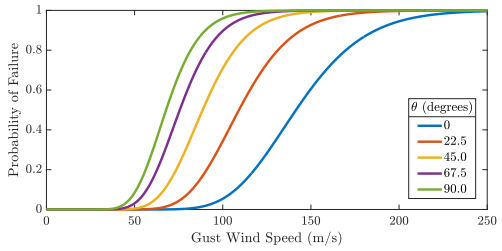

Fig. 2. Probability of wooden utility pole failure as a function of the three-second gust wind speed. Fragility curves are depicted given the pole parameters used in the case study for varying wind directions θ with respect to the conductor orientation.

The pump and line outage information is needed for running the hydraulic analysis (Section III-B) and solving for the power and water network resilience metrics (Section III-C).

B. Hydraulic Simulation

We simulate the water distribution network operation using the EPANET 2.2 hydraulic simulator within the WNTR (Water Network Tool for Resilience) package in Python [26]. EPANET is an open source hydraulic simulator that is commonly used by water utilities and researchers. Since we are considering cases where there may be low pressure levels and unmet water demands, we use the pressure-driven demand water flow analysis (as opposed to demand-driven water flow analysis which is only reasonable under normal operating conditions). Within WNTR, we run hydraulic simulations over all N scenarios for each operational control strategy.

C. Evaluating Operational Resilience

It is critical that the power and water distribution networks are able to anticipate, absorb, adapt to, and recover from disruptive events. Operational resilience is related to supply and demand availability, effectiveness of corrective actions, and the operational status of assets surrounding extreme events [15]. We use operational resilience metrics to quantify the performance of the power and water networks over the response and recovery to a hazard event [13], [27]. Resilience metrics capture network performance–such as loss of load and unmet water demand–over a specified time frame. For a given performance curve (such as the time-varying loss of load over the scheduling horizon), the associated network resilience metric R_n for scenario n is the relative network performance under a hazard event compared to normal operation over the scheduling horizon, i.e.,

$$R_n = \frac{\sum_{t\in\mathcal{T}} P^t_{\mathrm{W},n}}{\sum_{t\in\mathcal{T}} P^t_{\mathrm{N}}} \quad \forall\, n = 1...N, \quad (2)$$

where $P^t_{\mathrm{W},n}$ and P^t_{N} are the time-varying performance curves for the wind-induced outage scenario n and the normal operating case and $\mathcal{T}$ is the set of periods within the operational horizon. Note that the value R_n is normalized, where one indicates that the network performance is unaffected by the hazard event. Below, we describe different power and water network resilience metrics that can be used within resilience studies.

1) Power Distribution Network Resilience Metrics: For the power distribution network, we calculate resilience metrics on the number of active lines and connected loads in the wind-induced outage scenarios compared to the normal operating case

$$R_{\mathrm{line},n} = \frac{\sum_{t\in\mathcal{T}}\sum_{\ell\in\mathcal{L}} P^t_{\mathrm{line}\,\ell,\mathrm{W},n}}{\sum_{t\in\mathcal{T}}\sum_{\ell\in\mathcal{L}} P^t_{\mathrm{line}\,\ell,\mathrm{N}}} \quad \forall\, n = 1...N, \quad (3)$$

$$R_{\mathrm{load},n} = \frac{\sum_{t\in\mathcal{T}}\sum_{k\in\mathcal{K}} P^t_{\mathrm{load}\,k,\mathrm{W},n}}{\sum_{t\in\mathcal{T}}\sum_{k\in\mathcal{K}} P^t_{\mathrm{load}\,k,\mathrm{N}}} \quad \forall\, n = 1...N, \quad (4)$$

where $P^t_{\mathrm{line}\,\ell,\mathrm{W},n} \in \{0,1\}$ and $P^t_{\mathrm{load}\,k,\mathrm{W},n} \in \{0,1\}$ are the active/connected statuses of line ℓ and bus k at time t for

scenario n, $\mathcal{L}$ is the set of lines, and $\mathcal{K}$ is the set of buses. The variables $P^t_{\text{line }\ell,\text{N}} \in \{0,1\}$ and $P^t_{\text{load }k,\text{N}} \in \{0,1\}$ are the active/connected statuses of line ℓ and bus k at time t for the normal operating case. The power distribution network resilience metrics $R_{\text{line},n}$ and $R_{\text{load},n}$ quantify the severity of the wind events.

2) Water Distribution Network Resilience Metrics: For the water distribution network, we can quantify resilience in terms of the normalized water service availability $R_{\text{wsa},n}$ (i.e., the ratio of delivered water to expected water demand), pressure met $R_{\text{pressure},n}$ (i.e., demand junctions where the hydraulic head is above the minimum head limit $\underline{H}_j$), and the stored water capacity of the tank $R_{\text{tank},n}$ (i.e., ratio of water stored to cumulative tank volume) over the entire scheduling horizon for all scenarios n

$$R_{\text{wsa},n} = \frac{\sum_{t\in\mathcal{T}}\sum_{j\in\mathcal{J}} P^t_{\text{wsa }j,\text{W},n}}{\sum_{t\in\mathcal{T}}\sum_{j\in\mathcal{J}} P^t_{\text{wsa }j,\text{N}}} \quad \forall\, n = 1...N, \quad (5)$$

$$R_{\text{pressure},n} = \frac{\sum_{t\in\mathcal{T}}\sum_{j\in\mathcal{J}} P^t_{\text{pressure }j,\text{W},n}}{\sum_{t\in\mathcal{T}}\sum_{j\in\mathcal{J}} P^t_{\text{pressure }j,\text{N}}} \quad \forall\, n = 1...N, \quad (6)$$

$$R_{\text{tank},n} = \frac{\sum_{t\in\mathcal{T}}\sum_{j\in\mathcal{S}} P^t_{\text{tank }j,\text{W},n}}{\sum_{t\in\mathcal{T}}\sum_{j\in\mathcal{S}} P^t_{\text{tank }j,\text{N}}} \quad \forall\, n = 1...N, \quad (7)$$

where $P^t_{\text{wsa }j,\text{W},n}$ and $P^t_{\text{wsa }j,\text{N}}$ are the amounts of water received at junction j and time t for scenario n and the normal operating case, $P^t_{\text{pressure }j,\text{W},n}$ and $P^t_{\text{pressure }j,\text{N}}$ indicate whether the hydraulic head is within its operational limits at node j and time t for scenario n and the normal operating case, $P^t_{\text{tank }j,\text{W},n}$ and $P^t_{\text{tank }j,\text{N}}$ are the ratio of water volume to maximum tank volume at tank j and time t for scenario n and the normal operating case, $\mathcal{J}$ is the set of demand junctions, and $\mathcal{S}$ is the set of water storage tanks. It should be noted that variations in $R_{\text{tank},n}$ away from one are not necessarily bad; instead, the metric provides information on the ability of the tanks to supply and store water surrounding pump power outages.

IV. Optimal Water Pumping Frameworks

In this section, we summarize the network constraints and the problem formulation for the optimal water pumping problems. The problem is solved over set $\mathcal{T}$ with periods of duration ΔT. The water flow constraints are nonconvex, which makes the optimization problem difficult to solve, so we employ water flow approximations, resulting in a mixed-integer linear program (MILP) that we solve iteratively.

A. Modeling Water Flow Constraints

The water distribution network is represented as a directed graph with a set of nodes $\mathcal{N}$ and edges $\mathcal{E}$ connecting the nodes. Each node is classified as either a junction $\mathcal{J}$, reservoir $\mathcal{R}$, or storage tank $\mathcal{S}$. The edges are either pumps $\mathcal{P}$ or pipes (i.e., $\mathcal{E}\setminus\mathcal{P}$). The water flow at time t is characterized by the volumetric flow rate x^t_{ij} through pipe ij (i.e., from node i to node j) for all $ij \in \mathcal{E}$ and the hydraulic head H^t_j at node j for all $j \in \mathcal{N}$. The water flow constraints are summarized below.

1) Nodes: We first focus on the nodal constraints

$$\sum_{i:ij\in\mathcal{E}} x^t_{ij} + d^t_j = 0 \quad \forall\, j \in \mathcal{J}, \quad (8)$$

$$\underline{H}_j \le H^t_j \le \overline{H}_j \quad \forall\, j \in \mathcal{N}, \quad (9)$$

$$H^t_j = \widehat{h}_j \quad \forall\, j \in \mathcal{R}, \quad (10)$$

$$H^t_j = H^{t-1}_j - \frac{\Delta T}{\gamma_j} d^{t-1}_j \quad \forall\, j \in \mathcal{S}, \quad (11)$$

where d^t_j is the water injection at node j and time t, $\underline{H}_j$ and $\overline{H}_j$ are the minimum and maximum head limits at node j, and γ_j is the cross-sectional area of tank j. In (8), the conservation of water entering and exiting each junction must be satisfied. The hydraulic head (elevation plus pressure head) at all nodes must be within safe operating limits in (9). Reservoirs are modeled as infinite sources with a fixed hydraulic head $\widehat{h}_j$ in (10). In (11), the tank heads are updated given the previous period's head and tank water injection. Since the water demands follow a daily pattern, we want to ensure that the final tank levels over a 24-hour period are similar to the initial tank levels. We formulate the final cumulative tank levels with a soft constraint

$$\sum_{j\in\mathcal{S}} H^{t=0}_j \le s + \sum_{j\in\mathcal{S}} H^{t=24}_j \le \psi + \sum_{j\in\mathcal{S}} H^{t=0}_j, \quad (12)$$

where ψ is the water level tolerance and s is the cumulative tank level slack variable. Final tank levels outside of the tank level range (i.e., a non-zero s value) are penalized in the objective function. Formulating the final tank level limits as a soft constraint helps prevent feasibility issues in the iterative MILP formulation, which is presented in Section IV-A3.

2) Edges: We next describe the edge constraints. The hydraulic head at each node in the water network varies given the head loss along pipes and head gain across active pumps. The frictional head loss along a pipe is

$$H^t_i - H^t_j = k_{ij} \cdot x^t_{ij} \cdot |x^t_{ij}|^{\nu-1} \;\forall\, ij \in \mathcal{E}\setminus\mathcal{P}, \quad (13)$$

where k_{ij} is the pipe resistance coefficient of pipe ij and ν is the pipe head loss exponent. The general form of (13) can represent two common head loss formulas: Hazen-Williams and Darcy-Weisbach. In this work, we use the Hazen-Williams formula, where ν is 1.852 and k_{ij} is a function of pipe ij's length, diameter, and roughness coefficient. This is consistent with the head loss formula used within the WNTR simulator [26].

We next consider variable speed supply pumps, where w^t_{ij} is the normalized speed setting of pump $ij \in \mathcal{P}$ at time t and $z^t_{ij} \in \{0,1\}$ indicates whether pump $ij \in \mathcal{P}$ is on at time t

$$z^t_{ij} = 1 \Rightarrow H^t_j - H^t_i = b^0_{ij}(w^t_{ij})^2 + b^1_{ij}(x^t_{ij})^2 \;\forall\, ij \in \mathcal{P}, \quad (14)$$

$$\underline{w}_{ij} \cdot z^t_{ij} \le w^t_{ij} \le \overline{w}_{ij} \cdot z^t_{ij} \quad \forall\, ij \in \mathcal{P}, \quad (15)$$

$$0 \le x^t_{ij} \le \overline{x}_{ij} \cdot w^t_{ij} \quad \forall\, ij \in \mathcal{P}, \quad (16)$$

$$z^t_{ij} \in \{0,1\} \quad \forall\, ij \in \mathcal{P}, \quad (17)$$

where b^0_{ij} and b^1_{ij} are the nominal pump curve parameters of pump ij, $\underline{w}_{ij}$ and $\overline{w}_{ij}$ are the minimum and maximum pump speeds, and $\overline{x}_{ij}$ is the maximum pump flow rate when the pump is on and operating at the normalized pump speed.

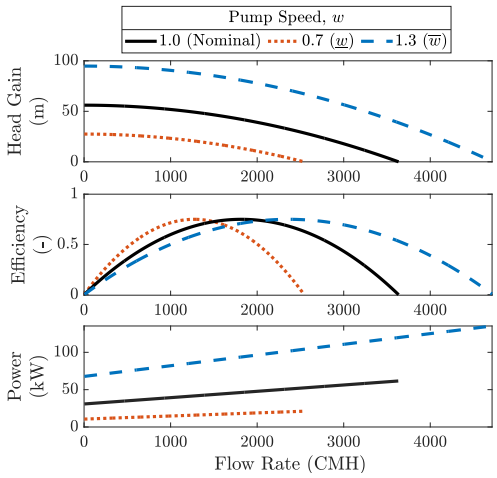

Fig. 3. Pump head gain (14), efficiency, and power consumption (19) for pump 1 in the case study. The solid black lines, the blue dashed lines, and the red dotted lines are the pump curves at nominal pump speed, maximum pump speed, and minimum pump speed, respectively.

In (14), we use an indicator constraint to formulate the pump head characteristics when the pump is on. When the pump is on (i.e., $z^t_{ij} = 1$), the power law models the head gain across the pump [28], [29]; when the pump is off, there is no flow through the pump and the head gain is arbitrary. Several off-the-shelf commercial solvers, such as Gurobi, have native support for indicator constraints. Alternatively, we can use the big-M method to formulate the on/off characteristics of the pump performance curve. The top plot of Fig. 3 illustrates how the pump head curve is adjusted at different pump speeds. When the pump is off, the flow rate and speed are zero (enforced by (15)-(16)). When the pump is on, the range of feasible flow rates in (16) scale with the pump speed (see Fig. 3). Specifically, the affinity laws approximate how changes in pump speed (i.e., pump speed w_1 to pump speed w_2) impact the pump characteristics [30], [31]

$$\frac{x_1}{x_2} = \frac{w_1}{w_2}, \qquad \frac{\hat{H}_1}{\hat{H}_2} = \left(\frac{w_1}{w_2}\right)^2, \qquad \frac{p_1}{p_2} = \left(\frac{w_1}{w_2}\right)^3, \tag{18}$$

where x, $\hat{H}$, and p represent the flow rate, head gain, and pump power, respectively. The subscripts '1' and '2' denote two different operating points.

The three-phase pump power consumption depends on the head gain and the flow rate across the pump as well as the pump efficiency. The pump efficiency—which is dependent on the pump flow rate and speed—is generally modeled with a quadratic or cubic polynomial [32]. We assume that the pumps are balanced three-phase loads with constant power factors. Fig. 3 illustrates the relationship between the flow rate and the pump's head gain, efficiency, and power consumption. The pump power consumption has a strong linear relationship with respect to the flow rate given a constant speed. The pump power consumption as a multivariable function of flow rate and speed can be approximated as

$$p^t_{ij} = c^0_{ij} \cdot (w^t_{ij})^2 + c^1_{ij} \cdot x^t_{ij} \cdot w^t_{ij} \quad \forall\, ij \in \mathcal{P}, \tag{19}$$

where c^0_{ij} and c^1_{ij} are parameters of the pump power consumption curve at nominal pump speed.

3) Approximation and Reformulation: The water flow constraints are mixed-integer nonconvex due to the pipe head loss (13), pump head gain (14), and pump power consumption (19) equations. To help with our reformulation, we define an intermediate variable $W^t_{ij} := (w^t_{ij})^2$ and use linear approximations for the head difference constraints that we update iteratively in the optimal pumping problem. We replace (13), (14)-(16), (19) with

$$H^t_i - H^t_j = f^{t,0}_{ij} + x^t_{ij} \quad \forall\, ij \in \mathcal{E}\backslash\mathcal{P}, \tag{20}$$

$$z^t_{ij} = 1 \Rightarrow H^t_j - H^t_i = b^0_{ij} W^t_{ij} + f^{t,1}_{ij} - x^t_{ij} \geq 0 \quad \forall\, ij \in \mathcal{P}, \tag{21}$$

$$(\underline{w}_{ij})^2 \cdot z^t_{ij} \leq W^t_{ij} \leq (\overline{w}_{ij})^2 \cdot z^t_{ij} \quad \forall\, ij \in \mathcal{P}, \tag{22}$$

$$0 \leq x^t_{ij} \leq \overline{x}_{ij} \cdot \overline{w}_{ij} \cdot z^t_{ij} \quad \forall\, ij \in \mathcal{P}, \tag{23}$$

$$p^t_{ij} = c^0_{ij} \cdot W^t_{ij} + c^1_{ij} \cdot x^t_{ij} \quad \forall\, ij \in \mathcal{P}, \tag{24}$$

where $f^{t,0}_{ij}$ and $f^{t,1}_{ij}$ are parameters. Instead of scaling the maximum pump flow rate by the pump speed, we restrict the pump head gain to be non-negative in (21) when the pump is on. This yields a MILP that we solve in an iterative fashion given updated parameters based on the flow rate x^t_{ij} of the previous solution, similar to [21]. During each iteration, the parameters are updated given the flow rate from the previous iteration

$$f^{t,0}_{ij} := x^t_{ij} \cdot (k_{ij} |x^t_{ij}|^{\nu-1} - 1) \qquad \forall\, ij \in \mathcal{E} \setminus \mathcal{P}, \tag{25}$$

$$f^{t,1}_{ij} := x^t_{ij} \cdot \left(b^1_{ij} x^t_{ij} + 1\right) \qquad \forall\, ij \in \mathcal{P}. \tag{26}$$

We recover the pump speed *a posteriori* by taking the square root of W^t_{ij}.

B. Optimal Water Flow Pumping Control (OWF)

We first present the OWF control strategy, where the water system operator minimizes the electricity costs of pumping subject to the water flow constraints and the water demand forecasts. The OWF problem is a MILP that we solve iteratively, where the steps are shown in Algorithm 1. The MILP problem solved during each iteration is

$$\min_{\mathbf{x}} \quad \sum_{t\in\mathcal{T}} \sum_{ij\in\mathcal{P}} \pi^t_{ij} \cdot p^t_{ij} \cdot \Delta T + c \cdot |s| \qquad \textbf{(OWF)}$$

$$\text{s.t.} \quad (8) - (11), (17), (20) - (24)\ \forall\, t \in \mathcal{T}, (12),$$

where the parameter π^t_{ij} is the cost of electricity at pump ij and time t and c is the penalty on the final tank level slack variable. The decision variable $\mathbf{x}$ is composed of the pump power consumptions p^t_{ij}, statuses z^t_{ij} , and speeds squared W^t_{ij} for all pumps $ij \in \mathcal{P}$ as well as the flow rates $x^t_{ij}\ \forall\ ij \in \mathcal{E}$, and hydraulic heads $H^t_j\ \forall\ j \in \mathcal{N}$ for all periods $t \in \mathcal{T}$. We update $\langle \boldsymbol{f} \rangle_k := \langle f^{t,0}_{ij}, f^{t,1}_{ij} \rangle_k$ given the flow rates from the previous iteration. We define the error as the Euclidean norm of the difference in $\langle \boldsymbol{f} \rangle_k$ between each consecutive iteration. We stop iterating when the error is below a certain threshold or we reach a maximum number of iterations. While there are no convergences guarantees, we found that the algorithm performed well with the daily tank level as a soft constraint. The absolute value $|s|$ in the objective function is reformulated using a non-negative slack variable.

Algorithm 1 Iterative OWF MILP Algorithm

Require: Water network topology, initial tank conditions $H_j^{t=0}\ \forall\ j \in \mathcal{S}$, and forecasted electricity prices $\pi_{ij}^t\ \forall\ ij \in \mathcal{P}, t \in \mathcal{T}$ and water demands $d_j^t\ \forall\ j \in \mathcal{J}, t \in \mathcal{T}$

Output: Pump power consumption p_{ij}^t, status z_{ij}^t, and speed $w_{ij}^t\ \forall\ ij \in \mathcal{P}, t \in \mathcal{T}$

Set $k \leftarrow 0$, tolerance, maxIter, and error
Initialize $\langle \boldsymbol{f} \rangle_k$ in (25)-(26), and $\langle \boldsymbol{x} \rangle_k$.
while error $\geq$ tolerance OR $k \leq$ maxIter **do**
  $k \leftarrow k + 1$
  Solve $(\text{OWF})_k$ using $\langle \boldsymbol{f} \rangle_{k-1}$ to obtain $\langle \boldsymbol{x}_{ij}^t \rangle_k$.
  Calculate $\langle \boldsymbol{f} \rangle_k$ given $\langle \boldsymbol{x}_{ij}^t \rangle_k$ in (25)-(26).
  Calculate error $:= ||\langle \boldsymbol{f} \rangle_k - \langle \boldsymbol{f} \rangle_{k-1}||_2$.
end while
The water system operator sets pump status $z_{ij}^t := \langle z_{ij}^t \rangle_k$ and speed $w_{ij}^t := \langle (W_{ij}^t)^{(1/2)} \rangle_k$.

C. Optimal Water Pumping Control + Frequency Regulation (OWF+FR)

We next present the OWF+FR control strategy, where the water system operator minimizes the cost associated with pump electricity consumption and the cost associated with providing frequency regulation capacity subject to the water flow constraints. To provide frequency regulation, the pumps track a frequency regulation signal sent by the independent system operator (which is updated on a seconds timescale) to balance real-time supply and demand mismatches. The water system operator solves for the optimal frequency regulation capacity in advance and then the pumps adjust their power consumption in real time as a function of the frequency regulation signal, i.e., $\widetilde{s} \in [-1, 1]$, which is biased by the schedule and scaled by the frequency regulation capacity. We assume a generator sign convention where up frequency regulation (a positive signal) corresponds to a decrease in pump power consumption and down frequency regulation (a negative signal) corresponds to an increase in pump power consumption.

In our formulation, we solve for the scheduled pump operation as well as the available frequency regulation capacity to adjust the pump power consumption given a frequency regulation signal. We assume that the water distribution network needs to be capable of providing the offered frequency regulation capacity over the entire hour time step t which is consistent with CAISO day-ahead market requirements for energy storage [33]. This ensures that the pumps can respond to the worst case signals (i.e., $+1$ or -1 for the entire hour). Additionally, we can use the same timescale as the quasi-steady state water flow constraints in our optimization problem. We assume that there is an offsetting mechanism so that the frequency regulation signal is 'energy neutral' over the contracted period [33]. We define F_{ij}^t as the maximum three-phase symmetric up and down frequency regulation capacity that pump ij can provide at time t

$$F_{ij}^t \geq 0 \quad \forall\ ij \in \mathcal{P}. \tag{27}$$

The OWF+FR problem is solved using the same iterative method as OWF, where the optimization problem solved in every iteration is

$$\begin{aligned} \min_{\mathbf{x}} \quad & \sum_{t \in \mathcal{T}} \sum_{ij \in \mathcal{P}} \pi_{ij}^t \cdot p_{ij}^t \cdot \Delta T - \pi_{\text{fr}}^t \cdot F_{ij}^t + c \cdot |s| \\ \text{s.t.} \quad & \mathcal{W}_{\text{scheduled}}(\boldsymbol{p}) \qquad \forall\ t \in \mathcal{T}, \qquad \textbf{(OWF+FR)} \\ & \mathcal{W}_{\text{FR}}(\boldsymbol{p} \pm \boldsymbol{F}),\ (27)\ \forall\ t \in \mathcal{T}, \end{aligned}$$

where π_{fr}^t is the expected price of frequency regulation capacity. The scheduled water flow constraint set $\mathcal{W}_{\text{scheduled}}(\cdot)$ contains (8)-(12), (17), (20)-(24). The constraint sets $\mathcal{W}_{\text{FR}}(\cdot)$ represent the water flow constraints if the full down and up frequency regulation was used, i.e., (8)-(11), (17), (20)-(24). The input $\boldsymbol{p} \pm \boldsymbol{F}$ is the power consumption when providing frequency regulation equal to the full frequency regulation capacity and replaces the left side of (24). The decision variable $\mathbf{x}$ includes the water flow variables associated with the schedule and frequency regulation capacity for all periods. The scheduled power consumption p_{ij}^t, speed w_{ij}^t, and frequency regulation capacities F_{ij}^t for each pump ij are solved for in the day-ahead optimization problem. The total frequency regulation capacity at time t is the cumulative capacity for all pumps at time t, i.e., $F^t = \sum_{ij \in \mathcal{P}} F_{ij}^t$. Unlike our previous work [5], which solves for the combined voltage support and frequency regulation capacity of fixed speed pumps as a mixed-integer second order cone program, the problem here is formulated as a MILP that solves for the frequency regulation capacity of variable speed pumps iteratively and the affinity laws are used to determine the real-time pump adjustments of variable speed pumps; this allows the problem to be solved quickly with nonlinear real-time adjustments. The iterative solution approach for solving the OWF+FR problem is similar to Algorithm 1, where we solve the (OWF+FR) problem at each iteration instead of the (OWF) problem. Once the problem converges, the water system operator also determines the frequency regulation capacity, F_{ij}^t.

The real-time pump power adjustments are determined by the affinity laws (18) given the frequency regulation signal $\widetilde{s}$

$$\hat{w}_{ij} = w_{ij}^t \cdot \left(1 + \frac{F_{ij}^t \widetilde{s}}{p_{ij}^t}\right)^{1/3} \qquad \forall\ ij \in \mathcal{P}, t \in \mathcal{T}, \tag{28}$$

where $\hat{w}_{ij}$ is the real-time pump speed. The scheduled pump speed w_{ij}^t, pump power consumption p_{ij}^t, and frequency regulation capacity F_{ij}^t are determined in (OWF+FR) for each period of ΔT. The real-time pump speed changes based on the frequency regulation signal on a faster time scale (e.g., every two seconds). This relationship applies when the pump is on and providing frequency regulation.

V. Case Study

In a case study, we compare power and water network resilience metrics given the optimal and rule-based pumping strategies under wind-induced power outages. We consider an interconnected power and water distribution network, with network topologies shown in Fig. 4. We consider a 72-hour time horizon.

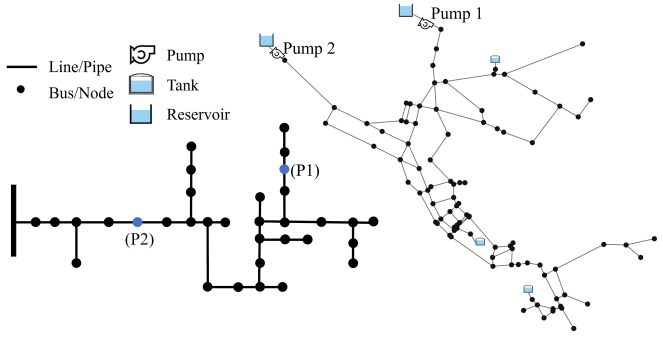

Fig. 4. Topology of the interconnected power distribution network (left) and water distribution network (right). Blue nodes in the power distribution network indicate the buses that have a pump connected.

A. Set Up

For the water distribution network, we use NET3, a 96-node example network included in the EPANET software. We set the minimum pressure head at the demand junctions to 20 psi and the maximum nominal pump flow to $\overline{x}_{ij} = (b^0_{ij}/b^1_{ij})^{1/2}\,\mathrm{m}^3/\mathrm{h}$ (same as the definition in WNTR). The pump curves are determined from EPANET's single-point curve definition given the desired flow rate and head at nominal speed provided in the EPANET INP file. The minimum and maximum normalized pump speeds are 0.7 and 1.3, respectively. In [31], the authors found that for speed changes less than 33% of the nominal speed, the affinity laws accurately approximate pump performance and changes in the pump efficiency curve can be neglected. We use cubic pump efficiency functions developed in [32], where the peak wire-to-water efficiency of both pumps is 75%.

For the power distribution network, we use the IEEE 34-node test feeder [34]. We assume that all of the utility poles are 50-year old class five poles; class five distribution poles are typically used in the United States [35]. We assume a span length of 46 meters, $A_c = 2$ m^2, and height of 12.2 meters. The pumps are connected to buses 844 and 814. The electricity price is shown in Fig. 5a. We set the frequency regulation capacity price to $\$0.20/\mathrm{kW}$ and assume it is known in advance.

For the wind-based hazard, we assume the three-second gust wind speed is spatially uniform (yet with temporal variations) over the feeder, with an event duration of five hours (see Fig. 5b). To consider different storm intensities, we use a multiplier to scale the three-second wind gust speed, e.g., a 150% wind speed intensity indicates that the wind speeds in Fig. 5b are multiplied by 1.5. The wind direction is 30° from due east. It should be noted that the orientation of each conductor with respect to the wind direction determines the 'steepness' of the fragility curve. The probability of failure is higher at smaller wind speeds when the angle between the wind and conductor is larger (see Fig. 2). There can be multiple pole outages that impact the outage of a power distribution line. The active time to repair each pole is five hours [27]. We consider five crews repairing the utility poles in order of priority. It is assumed that no repairs are made during the storm for safety purposes. Therefore, the repairs start at the end of the wind event. The wind event start time is randomly

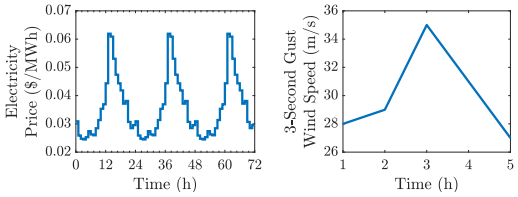

Fig. 5. (Left) Electricity prices over scheduling horizon and (Right) Nominal three-second wind gust speed during the wind hazard event.

generated from a uniform distribution U$[t = 9, t = 19]$ to ensure that the entire wind event concludes in the first 24 hours. We consider a sample size of $N = 500$ scenarios, where we also evaluate the impact of sample size in Section V-B5.

For the hydraulic simulation, we use the EPANET 2.2 simulator within the WNTR v.1.0.0 Python package [26]. For all control strategies in our case study, we assume the water network reverts to rule-based control when the water distribution network experiences an outage. While we could also update the optimal water pumping problem given a partial outage or restoration, we do not have information on how the water system operator would make changes to the rule-based operation during and after an outage event. As a result, the only aspect that changes between simulations in our case study is what strategy is used before the outage occurs. For the rule-based control strategy, we use the pre-existing controls in NET3's input file. For the optimal control strategies, we add a condition so that the WNTR rule-based controls are not used under normal conditions (i.e., before any pump outages occur). This is done by rewriting the WNTR controls as rules with an additional simulation time condition. We use a hydraulic time step and reporting time step of two seconds to be consistent with the frequency regulation signal. With the optimal control strategies, we set the pump speed and status using simulation time condition rules. For the frequency regulation signal within the real-time simulation, we use PJM's RegD signal from January 1, 2020 [36]. We use the EPANET simulator within the WNTR package instead of the WNTR simulator since the WNTR simulator is missing features necessary for our hydraulic analysis (e.g., the WNTR simulator cannot accommodate variable speed pumps). The EPANET simulator has an issue where the tanks can still supply water to the network when the tanks are empty resulting in incorrectly reported supplied water values and pressure values. We can estimate the actual water service ability by subtracting the (fictional) amount of water that is supplied to the network by the tanks at their minimum water level from the EPANET simulator's reported supplied water demand. To verify the accuracy of this approach, we compare the water service availability calculated *a posteriori* with the EPANET solver with the water service availability calculated with the WNTR simulator for a fixed speed pump case. We found that the water service availability is very similar between the two approaches (i.e., 35.76% versus 35.56%).

We solve the OWF and OWF+FR problems using Gurobi v9.5.2 in the JuMP package in Julia over the scheduling horizon. We initialize the iterative algorithms with the rule-based schedule. We set the tank violation penalty c to 10,000 in order to maintain feasibility within the successive iterations

TABLE I
DAILY OPERATIONAL COSTS UNDER NORMAL OPERATION

Control Strategy	Electricity Cost ($)	Frequency Regulation Profit ($)	Total Costs ($)
(Rule)	208.02	-	208.02
(OWF)	83.59	-	83.59
(OWF+FR)	107.55	44.91	62.64

of Algorithm 1 while discouraging final tank levels outside our desired range. We set ψ to 2 m.

B. Results

1) Performance of Water Network Operation Strategies under Normal Operation: We first compare the three control strategies under normal operation using the EPANET simulator. Figure 6 depicts the tank levels and pump power consumption for each control strategy. Due to the diurnal pattern of water demands and the operational constraint that ensures the tank levels at the start of each day are similar (12), the normal operation for the three days within the scheduling horizon is very similar. Although we consider a 72-hour time horizon for both normal and extreme operations, we show the results for the normal operating conditions over a 24-hour time horizon. The pump power consumption between the control strategies ends up varying significantly. In the rule-based control, pump 1 switches on and off frequently. This is because the rule-based operation has stricter constraints on the tank level: a control rule enforces that pump 1 is turned on whenever tank 1's water level goes below 40% and continues pumping until tank 1's water level goes above 60% of its total available capacity. In the optimal control strategies, the pump speed varies away from the normalized pump speed in order to realize lower costs and/or provide frequency regulation. In the OWF+FR case, very frequent pump power changes occur during periods where the pump is providing frequency regulation. Frequent pump power adjustments are made as the pumps change their speeds to track the frequency regulation signal. The pumps do not always provide frequency regulation. In the OWF+FR case in Fig. 6, the optimization problem determines that it is most cost-effective for the water distribution network to provide frequency regulation for seven time periods within the scheduling horizon. During the other periods, the pumps are operating at their minimum pump speed $\underline{w}_{ij}$ and are unable to provide up frequency regulation (i.e., decrease pump power consumption from their scheduled set point). Since the pumps must provide symmetric up and down frequency regulation, this prevents the pumps from providing frequency regulation during these time periods. We calculate the average tank level over the scheduling horizon as 64.1%, 56.3%, and 58.4% for the rule-based, OWF, and OWF+FR cases, respectively. This indicates that the rule-based operation keeps the tank fuller during each 24-hour period. We also can observe that the optimal tank level is higher when providing frequency regulation, likely because there needs to be enough water in the tanks for the pumps to provide both up and down frequency regulation.

Table I reports the electricity costs, frequency regulation profit, and total costs for the three control strategies. We

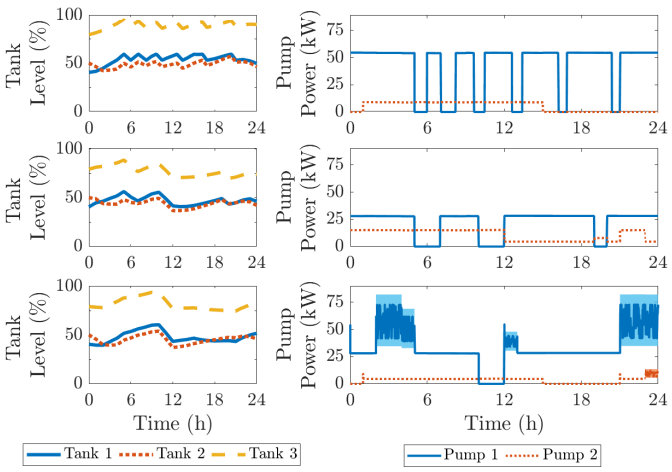

Fig. 6. (Left) Tank water levels as percentage of total operational tank volume, and (Right) pump power consumption in the Rule-based (top), OWF (middle), and OWF+FR (bottom) control strategies under normal operating conditions. The lightly shaded blue and red bands in the OWF+FR's pump power consumption plot (bottom right) illustrates the frequency regulation capacity for pumps 1 and 2, respectively.

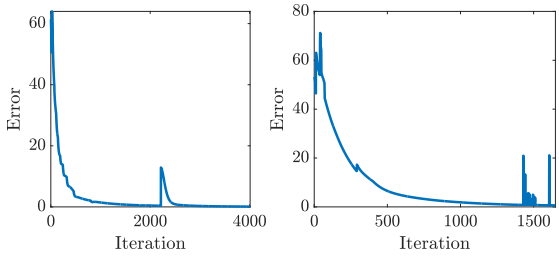

Fig. 7. Convergence of the OWF (left) and OWF+FR (right) iterative solution approaches.

observe that the total costs of the optimal control strategies are significantly less than the rule-based control strategy. For instance, the costs of the OWF and OWF+FR solutions are 59.8% and 69.9% less than the rule-based solution cost. This is because the optimal pumping strategies minimize the electricity cost associated with pumping and, in the OWF+FR problem, maximizes profit associated with frequency regulation.

2) Accuracy and Performance of Solution Approach: We next evaluate the accuracy and performance of the optimal pumping strategies within the two-second resolution hydraulic simulator under normal operation. All control strategy solutions were feasible where the hydraulic heads, pump flow rates, and tank levels were within the specified limits. Additionally, the final tank levels were similar to the initial tank levels (see Fig. 6). The OWF and OWF+FR problem converged in 4011 and 1649 iterations, respectively. Fig. 7 shows the iteration error for the OWF and OWF+FR problem. While there are no guarantees of convergence, we found that the approach performed well. The solver time for the MILP iteration was less than a tenth of a second for the OWF problem and 2 seconds for the OWF+FR problem on a 64-bit Intel i7 core CPU at 2.10 GHz and 32-GB RAM.

Figure 8 illustrates the water pumps' ability to follow the frequency regulation signal with the OWF+FR control

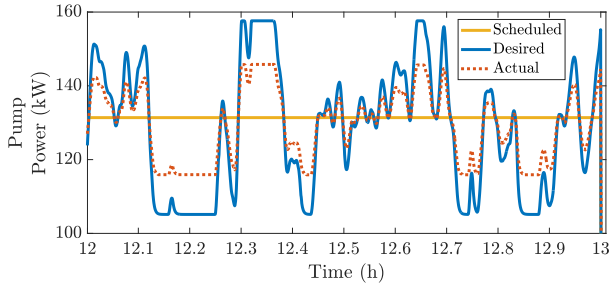

Fig. 8. Frequency regulation performance over one hour within the OWF+FR problem. The blue solid line is the expected pump power consumption given the frequency regulation signal. The red dashed line is the actual pump power consumption simulated in WNTR. The yellow solid line is the scheduled, or nominal, pump schedule.

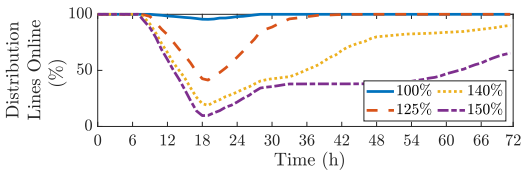

Fig. 9. Percentage of power distribution lines online for varying wind speed intensities. Each curve is the average performance curve over 500 scenarios.

strategy. We examine the OWF+FR control strategy over the span of one hour to better observe the pump adjustments made based on the two-second frequency regulation signal. It should be noted that other time periods in which the pumps provide frequency regulation have a similar performance. We calculate the real-time pump speed in (28) given the frequency regulation signal and the optimal frequency regulation capacity, scheduled pump speed, and scheduled pump power consumption solved for in (OWF+FR). Overall, we observe that the pumps generally follow the frequency regulation signal but the affinity laws appear to consistently over-estimate the real-time pump power deviation that is provided. It should be noted that the affinity laws are an approximation of the change in pump curves. The actual pump set point is determined given the intersection of the pump head curve and the system curve. However, when we calculated PJM's performance score using [37], the pump performance was sufficient. To minimize the signal error further, we could alternatively use real-time feedback of the pump power consumption to adjust the pump speed instead of using the affinity laws (e.g., with a proportional-integral controller).

3) Resilience of Power Network Surrounding Wind Hazard Events: Next, we consider the impact of the wind hazard on the power distribution network. We calculate the averaged resilience metrics of the active distribution lines $R_{\text{lines},n}$ and connected loads $R_{\text{load},n}$ (using the definitions in (3) and (4)) over all scenarios n and report the results in Table II. As expected, the loss in loads and lines increases as the wind speed intensity increases. The power distribution network performance curves help us understand the implications of storm severity over time. To illustrate, in Fig. 9, we plot the active line performance curves of the power distribution network, averaged over 500 scenarios, while varying the three-second wind gust speed intensity. In Fig. 9, we can observe that

TABLE II
AVERAGE POWER DISTRIBUTION NETWORK RESILIENCE METRICS

Wind Speed (%)	R_{load} (%)	R_{lines} (%)
100	99.22	99.38
125	87.54	89.78
140	59.37	67.42
150	39.27	47.90

TABLE III
AVERAGE WATER DISTRIBUTION NETWORK RESILIENCE METRICS

Wind	R_{wsa} (%)			R_{tank} (%)		
Speed	Rule	OWF	OWF+FR	Rule	OWF	OWF+FR
100	99.91	99.89	99.85	98.35	99.08	93.20
125	97.31	96.54	96.51	75.98	58.58	73.36
140	77.83	73.17	77.58	47.74	36.92	45.82
150	46.49	37.66	47.06	24.76	25.16	22.71

the recovery time of the 140% and 150% wind intensities is significantly longer than the 100% and 125% wind intensities.

4) Resilience of Water Network Surrounding Wind Hazard Events: We next evaluate the resilience of the rule-based, OWF, and OWF+FR control strategies when the water distribution network is experiencing pump outages due to a wind hazard. Table III presents the resilience of the rule-based, OWF, and OWF+FR control strategies for varying wind speed intensities. We calculate the average resilience metrics for $R_{\text{wsa},n}$ and $R_{\text{tank},n}$ over all scenarios n using the definitions in (5) and (7). We do not compute $R_{\text{pressure},n}$ because of limitations with the EPANET simulator, which are discussed in Section V-A. As expected, the resilience of the water distribution network decreases as the wind hazard intensity increases. The water availability between control strategies is close but generally worse in the optimal control strategies compared to the rule-based strategy. We also observe that tank levels are more depleted in the optimal control strategies.

One thing to note is that the controls in the rule-based strategy keep the tank levels within a smaller range of possible values (e.g., a control rule enforces tank 1's water storage to be between 40% and 60% of the total operational tank capacity). Alternatively, the optimal pumping problems do not place further limits on the tank levels throughout the scheduling horizon. Since the optimal pumping strategies choose less expensive operating points, there is a chance that the operational set points may end up being more risky for the water distribution network. To address this, we can incorporate constraints within the optimal pumping problem to improve the water network resilience. For example, we could strictly limit the scheduled tank level operation to be within a restricted range of values or penalize deviations outside of a certain range of tank levels. In the case where the water system operator is aware of an upcoming hazard event, pre-filling tank constraints can be incorporated into the optimal pumping problem, as is often done in practice.

To illustrate this, we investigate the impact of adding a minimum tank level constraint to the OWF control strategy. We choose the OWF control strategy since the resilience metrics were generally lowest for this strategy. We enforce that tank 1's water storage must be greater than or equal to 45% capacity. In Table IV, the resilience metrics are presented for the modified OWF control strategy. As expected, when we constrain the

TABLE IV
AVERAGE RESILIENCE METRICS FOR MODIFIED OWF

Wind Speed	R_{wsa} (%)	R_{tank} (%)
100	99.94	100.00
125	97.34	64.19
140	74.36	40.58
150	38.88	28.65

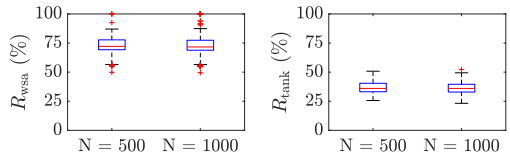

Fig. 10. Box plots of the OWF solution's $R_{\text{wsa},n}$ (left) and $R_{\text{tank},n}$ (right) resilience metrics for 500 and 1000 scenarios with 140% wind intensity.

lower limits of tank 1, we see that the resilience of the water distribution network increases. In this case, we still observe that the resilience metrics are lower than in the rule-based scenario. This is because the rule-based strategy requires that pump 1 remains on until tank 1 is at 60% capacity, whereas the OWF strategy just enforces a lower limit for the tank level.

In all cases, pump outages deplete the tanks. This is because the tanks provide more water to meet demand when the pumps cannot. For short periods, tanks can be used to hedge against outages and water demand uncertainty. The OWF+FR control strategy generally performs better than the OWF control strategy and comparable to the rule-based strategy. This is likely due to the OWF+FR schedule maintaining a more conservative set point in which the tank levels vary less in order to be able to respond to both up and down frequency regulation. Consequently, while the scheduled electricity cost in the OWF+FR solution is higher than the cost in the OWF solution (see Table I), using the water pumps to supply frequency regulation decreases total costs and can help hedge the water distribution network against hazards.

5) Impact of Scenario Sample Size on the Resilience Metrics: Lastly, we evaluate whether we get representative results when using a sample size of 500 scenarios. To do this, we re-run all of the hydraulic simulations of the rule-based, OWF, and OWF+FR control strategies using 1,000 scenarios and compare the characteristic mean and standard deviations for these two sample sets. Fig. 10 compares the distribution of the resilience metrics over the two sample sets. Overall, the mean and standard deviation of the water distribution network resilience metrics $R_{\text{wsa},n}$ and $R_{\text{tank},n}$ across 500 scenarios and 1000 scenarios are close. This indicates that the resilience results calculated using 500 scenarios are representative of the actual resilience of the control strategies.

VI. CONCLUSION

In this paper, we evaluate the ability of water pumps in the water distribution network to provide frequency regulation services to the bulk transmission system given wind hazard events. We compare the performance and operational resilience of the water network given a wind-based event under different control strategies. The wind event causes power outages in the power distribution network which then causes pump outages in the water distribution network. We find that the cost of the optimal strategies are significantly less expensive than the traditional, heuristic approach (i.e., with cost reductions greater than 59%). When simulating the wind-based hazards, the optimal strategies performed worse since less water demand was supplied and the tank levels remained at lower levels than the rule-based control. This is due to the fact that the rule-based control strategy has stricter tank limits during normal operation than what is included in the optimal water flow problem. However, we can incorporate constraints that can improve the network resilience (e.g., tank limits throughout the scheduling horizon or tank pre-filling requirements before a big storm).

Furthermore, we observe that operational resilience improves when the water network provides frequency regulation (OWF+FR) compared to just minimizing electricity costs, since the frequency regulation service helps buffer the tank levels. This indicates that allocating reserve capacity to frequency regulation may also help provide a buffer in water distribution network operation against hazards. Future work will implement methods to eliminate error in the frequency regulation response (i.e., a feedback controller), develop metrics to capture other significant aspects of performance, such as water quality and pressure met, investigate performance on more water distribution networks as well as consider network simplification approaches (e.g. [38]), and evaluate trade-offs between operational costs and long-term concerns of wear-and-tear on the pumps due to more frequent pump changes.

REFERENCES

[1] K. S. Ayyagari, S. Wang, N. Gatsis, A. F. Taha, and M. Giacomoni, "Co-optimization of interdependent water and power distribution networks," *IEEE PES Innov. Smart Grid Technol. (ISGT)*, 2021.
[2] D. Fooladivanda, A. D. Dominguez-Garcia, and P. Sauer, "Utilization of water supply networks for harvesting renewable energy," *IEEE Trans. Control Netw. Syst.*, vol. 6, no. 2, pp. 763 – 774, 2019.
[3] A. Zamzam, E. Dall'Anese, C. Zhao, J. Taylor, and N. Sidiropoulos, "Optimal water-power flow problem: formulation and distributed optimal solution," *IEEE Trans. Control Netw. Syst.*, vol. 6, no. 1, pp. 37–47, 2019.
[4] M. K. Singh and V. Kekatos, "Optimal scheduling of water distribution systems," *IEEE Trans. Control Netw. Syst.*, vol. 7, no. 2, pp. 711–723, 2020.
[5] A. Stuhlmacher and J. L. Mathieu, "Flexible drinking water pumping to provide multiple grid services," *Electr. Power Syst. Res.*, vol. 212, p. 108491, 2022.
[6] A. Stuhlmacher and J. L. Mathieu, "Chance-constrained water pumping to manage water and power demand uncertainty in distribution networks," *Proc. IEEE*, vol. 108, no. 9, pp. 1640 – 1655, 2020.
[7] S. Zuloaga, P. Khatavkar, V. Vittal, and L. W. Mays, "Interdependent electric and water infrastructure modelling, optimisation and control," *IET Energy Systems Integration*, vol. 2, no. 1, pp. 9–21, 2020.
[8] A. Belmondo Bianchi, M. A. Pardo, T. Alskaif, H. H. M. Rijnaarts, and S. Shariat Torbaghan, "Novel market-based mechanism for flexibility provision by water distribution networks to power systems," *IEEE Access*, vol. 12, pp. 86869–86885, 2024.
[9] I. Boukas, E. Burtin, A. Sutera, Q. Gemine, B. Pevee, and D. Ernst, "Exploiting the flexibility potential of water distribution networks: A pilot project in belgium," *IEEE Trans. Smart Grid*, vol. 15, no. 1, pp. 394–404, 2024.
[10] A. Farahmand-Zahed, A. Akbari-Dibavar, B. Mohammadi-Ivatloo, and K. Zare, "Optimal Scheduling of Water Distribution Systems' Participation in Demand Response and Frequency Regulation Services," in *Electricity Markets: New Players and Pricing Uncertainties* (S. Nojavan and K. Zare, eds.), pp. 213–228, Springer International Publishing, 2020.
[11] M. Duffy, "Creating operational efficiencies in the water industry," tech. rep., American Water, 2014.

[12] A. Stuhlmacher and J. L. Mathieu, "Demand response potential of drinking water distribution networks," in *Proc. Hawaii International Conference on System Sciences (HICSS)*, 2025.
[13] M. Panteli, P. Mancarella, D. N. Trakas, E. Kyriakides, and N. D. Hatziargyriou, "Metrics and quantification of operational and infrastructure resilience in power systems," *IEEE Trans. Power Syst.*, vol. 32, no. 6, pp. 4732–4742, 2017.
[14] S. Chanda, A. K. Srivastava, M. U. Mohanpurkar, and R. Hovsapian, "Quantifying power distribution system resiliency using code-based metric," *IEEE Trans. Ind. Appl.*, vol. 54, no. 4, pp. 3676–3686, 2018.
[15] G. V. Iswaran, R. Vakili, and M. Khorsand, "A comprehensive framework based on dynamic and steady state analysis to evaluate power system resiliency to extreme weather conditions," *Proc. IREP Bulk Power System Dynamics and Control*, 2022.
[16] K. A. Klise, R. Murray, and L. T. N. Walker, "Systems measures of water distribution system resilience," Tech. Rep. EPA/600/R-14/383, U.S. EPA Office of Research and Development, 2015.
[17] S. Zuloaga and V. Vittal, "Quantifying power system operational and infrastructural resilience under extreme conditions within a water-energy nexus framework," *IEEE Open Access J. Power Energy*, vol. 8, pp. 229–238, 2021.
[18] S. Zuloaga, P. Khatavkar, L. Mays, and V. Vittal, "Resilience of cyber-enabled electrical energy and water distribution systems considering infrastructural robustness under conditions of limited water and/or energy availability," *IEEE Trans. Eng. Manag.*, vol. 69, no. 3, pp. 639–655, 2022.
[19] L. Rodriguez-Garcia, M. M. Hosseini, T. M. Mosier, and M. Parvania, "Resilience analytics for interdependent power and water distribution systems," *IEEE Trans. Power Syst.*, vol. 37, no. 6, pp. 4244–4257, 2022.
[20] K. Oikonomou, M. Parvania, and R. Khatami, "Optimal Demand Response Scheduling for Water Distribution Systems," *IEEE Trans. Ind. Electron.*, vol. 14, no. 11, pp. 5112–5122, 2018.
[21] K. S. Ayyagari and N. Gatsis, "Optimal pump scheduling in multi-phase distribution networks using benders decomposition," *Electr. Power Syst. Res.*, vol. 212, p. 108584, 2022.
[22] J. H. Eto, K. H. LaCommare, P. Larsen, A. Todd, and E. Fisher, "An examination of temporal trends in electricity reliability based on reports from U.S. electric utilities," Tech. Rep. LBNL-5268E, Lawrence Berkeley National Laboratory, 2012.
[23] R. Goldstein and W. Smith, "Water & sustainability (volume 4): US electricity consumption for water supply & treatment-The next half century," Tech. Rep. 1006787, EPRI, 2002.
[24] B. Anderson, A. Schumacher, S. Guikema, S. Quiring, J. Ferreri, A. Staid, M. Guo, L. Ming, and L. Zhu, "stormwindmodel." https://github.com/geanders/stormwindmodel, 2018.
[25] Y. M. Darestani and A. Shafieezadeh, "Multi-dimensional wind fragility functions for wood utility poles," *Eng. Struct.*, vol. 183, pp. 937–948, 2019.
[26] K. A. Klise, D. Hart, D. M. Moriarty, M. L. Bynum, R. Murray, J. Burkhardt, and T. Haxton, "Water network tool for resilience (WNTR) user manual," Tech. Rep. EPA/600/R-20/185, U.S. EPA Office of Research and Development, 2020.
[27] M. Ouyang and L. Dueñas Osorio, "Multi-dimensional hurricane resilience assessment of electric power systems," *Struct. Saf.*, vol. 48, pp. 15–24, 2014.
[28] L. A. Rossman, H. Woo, M. T. F. Shang, R. Janke, and T. Haxton, "EPANET 2.2 User Manual," Tech. Rep. EPA/600/R-20/133, U.S. Environmental Protection Agency, 2020.
[29] C. D'Ambrosio, A. Lodi, S. Wiese, and C. Bragalli, "Mathematical programming techniques in water network optimization," *Eur. J. Oper. Res.*, vol. 243, no. 3, pp. 774–788, 2015.
[30] A. Marchi, A. R. Simpson, and N. Ertugrul, "Assessing variable speed pump efficiency in water distribution systems," *Drink. Water Eng. Sci.*, vol. 5, no. 1, pp. 15–21, 2012.
[31] I. Sárbu and I. Borza, "Energetic optimization of water pumping in distribution systems," *Period. Polytech. Mech. Eng.*, vol. 42, no. 2, pp. 141–152, 1998.
[32] B. Ulanicki, J. Kahler, and B. Coulbeck, "Modeling the efficiency and power characteristics of a pump group," *J. Water Resour. Plan. Manag.*, vol. 134, no. 1, pp. 88–93, 2008.
[33] California ISO, "Regulation energy management draft final proposal." https://www.caiso.com/Documents/RevisedDraftFinalProposal-RegulationEnergyManagement-Jan13_2011.pdf, 2011.
[34] W. H. Kersting, "Radial distribution test feeders," *Proc. IEEE Power Eng. Soc. Winter Meet.*, vol. 2, pp. 908–912, 2001.
[35] C. Zhai, T. Y.-j. Chen, A. G. White, and S. D. Guikema, "Power outage prediction for natural hazards using synthetic power distribution systems," *Reliab. Eng. Syst. Saf.*, vol. 208, p. 107348, 2021.
[36] PJM, "Ancillary services: RTO regulation signal data." https://www.pjm.com/markets-and-operations/ancillary-services. Accessed: 2022-12-13.
[37] G. S. Ledva, I. M. Granitsas, O. Oyefeso, S. A. Nugroho, P. Phanivong, I. A. Hiskens, and J. L. Mathieu, "Co-simulation testbed and controllers for compressor-based loads providing grid balancing services." https://github.com/Giannisgran/Co-Simulation-testbed-and-controllers-for-compressor-based-loads-providing-grid-balancing-services, 2023.
[38] F. J. Martínez-Solano, P. L. Iglesias-Rey, D. Mora-Meliá, and V. S. Fuertes-Miquel, "Exact Skeletonization Method in Water Distribution Systems for Hydraulic and Quality Models," *Procedia Engineering*, vol. 186, pp. 286–293, 2017.

Anna Stuhlmacher (Member, IEEE) is an Assistant Professor in the Electrical and Computer Engineering Department at Michigan Technological University, Houghton, MI, USA. She received the B.S. degree in electrical engineering from Boston University, Boston, MA, USA, in 2017, and the M.S. and Ph.D. degrees in electrical engineering from the University of Michigan, Ann Arbor, MI, USA, in 2019 and 2023, respectively. Her research interests include the optimization of uncertain distributed energy resources and the coordination of the power grid with other infrastructure systems, such as drinking water and agricultural systems.

Seth Guikema is a Professor in the Civil and Environmental Engineering and Industrial and Operations Engineering departments at the University of Michigan and a Professor II in the Department of Safety, Economics, and Planning at the University of Stavanger. He received a B.S. in Environmental Engineering from Cornell University (1997), M.S. in Civil and Environmental Engineering from Stanford University (1999), M.Eng by thesis in Civil Engineering from the University of Canterbury (1999), and Ph.D. in Engineering Risk and Decision Analysis from Stanford University (2003). He has also served as a faculty member at Texas A&M University, a faculty member at Johns Hopkins University, a Senior Analyst with Innovative Decisions, Inc. and a Data Science Fellow at One Concern, Inc.

Johanna L. Mathieu (Senior Member, IEEE) received the B.S. degree in ocean engineering from the Massachusetts Institute of Technology, Cambridge, MA, USA, in 2004 and the M.S. and Ph.D. degrees in mechanical engineering from the University of California, Berkeley, USA, in 2008 and 2012, respectively. She is an Associate Professor in the Department of Electrical Engineering and Computer Science at the University of Michigan, Ann Arbor, MI, USA. Prior to joining the University of Michigan, she was a postdoctoral researcher at the Swiss Federal Institute of Technology (ETH) Zurich, Switzerland. Her research interests include modeling, estimation, control, and optimization of distributed energy resources.